Jurnal Tribologi 31 (2021) 28-45

MYTRIBOS Malaysian Tribology Society

Jurnal Tribologi

Website : jurnaltribologi.mytribos.org e-issn: 2289-7232

Temperature distribution in a drilling brake contact

Fikrat Yusubov *, Alasgar Aliyev

Department of Mechanics, Azerbaijan State Oil and Industry University, AZERBAIJAN.
*Corresponding author: fikratyusub@gmail.com

KEYWORDS

Frictional heat
FEM model
Drilling
Brake contact
Simulation

ABSTRACT

The hoisting system of the drilling rig, equipped with drawworks, performs important operations such as lifting and lowering the drill pipes into the well. During repetitive braking, thermal heat is generated due to the friction between the contact area of the brake disk and pads. Most part of the generated heat is absorbed by the brake drum and another part is shared between the disk and pads. The main purpose of this paper is to study the heat distribution of the disk and pad during the braking period. Heat generation and dissipation mechanism in contact of asbestos–based brake friction composite and 35HNL steel disk material were studied. The geometric dimensions of the brake system of the drilling rig type ZJ30 were used as a prototype. Heat model and analysis are done using the "Heat transfer in solids (ht)" module via COMSOL Multiphysics 5.5 software. The finite element simulations helped to determine the temperature distribution on the contact surface over the selected braking time. The results show that the highest surface temperature was observed first 2-4 secs of the braking phase according to the given parameters.

Received 13 April 2021; received in revised form 6 July 2021; accepted 6 November 2021.
To cite this article: Yusubov et al. (2021). Temperature distribution in a drilling brake contact. Jurnal Tribologi 31, pp.28-45.

NOMENCLATURES

T	Temperature, K
ρ	Density, kg/m^3
R_1	Inner radius, m
R_2	Outer radius, m
α_1	Heat transfer coefficient of the outer surface of the brake disc, W/(m^2·K)
α_2	Heat transfer coefficient of the inner surface of the brake disc, W/(m^2·K)
t_T	Braking time, sec
T_0	Enviromental temperature, K
T_1	Initial temperature, K
P_b	Frictional heat source
μ	Friction coefficient
v	Sliding velocity, m/s
ω	Angular velocity, rad/s
R	Radius, m
ρ	Density, kg/m^3
C_p	Specific heat capacity at constant stress, J/kg·K
T	Absolute temperature, K
u_{trans}	Velocity vector of translational motion, m/s
q	Heat flux by conduction, W/m^2
q_r	Heat flux by radiation, W/m^2
Q	Additional heat sources, W/m^3
Q_{ted}	Thermoelastic damping, W/m^3
α	Coefficient of thermal expansion, 1/K
S	Second Piola-Kirchhoff stress tensor, Pa
n	Normal vector on the boundary
q	Conductive heat flux vector, W/m^2
k	Thermal conductivity, W/(m·K)
∇T	Temperature gradient, K/m
q_0	Inward heat flux, W/m^2
h	Heat transfer coefficient
T_{ext}	External temperature, K
Pr	Prandtl number
Re_L	Reynolds number, W/(m·K)
n	Normal vector toward exterior
L	Radius or length of the cylinder, m
n	Normal vector toward exterior
T_d	Downside temperature, K
T_u	Upside temperature, K
Q_b	Boundary heat source, W/m^2
q_d	Downside heat flux, W/m^2
q_u	Upside heat flux, W/m^2
h	Local average heat-transfer coefficient
r	Heat partition coefficient
ξ	Martensite state volume fraction
$C_{p,u}$	Upside specific heat capacity, respectively, J/kg·K
$C_{p,d}$	Downside specific heat capacity, respectively, J/kg·K

n_u Normal vector toward exterior for upside partition
n_d Normal vector toward exterior for downside partition
ρ_u Upside density, kg/m^3
ρ_d Downside density, kg/m^3
k_u Upside thermal conductivity, W/m·K
k_d Downside thermal conductivity, W/m·K
Q_1 Produced heat, W/m^3
Q_2 Dissipated heat, W/m^3
W_1 Total heat rate, correspondending to Q_1, J
W_2 Total heat rate correspondending to Q_2 , J
h Joint conductance, W/m^2·K
h_c Constriction conductance, W/m^2·K
h_g Gap conductance, W/m^2·K
h_r Radiative conductance, W/m^2·K
$k_{contact}$ Harmonic mean of the contacting surface conductivities, Wt/m·K
m_{asp} Asperities average slope, m
σ_{asp} Asperities average height, m
H_C Microhardness, Pa
ε Surface emissivity, σ Stefan-Boltzmann constant, W/m$^{2\cdot}$K^4
T_{amb} Enviromental temperature, K

1.0 INTRODUCTION

The first operation to extract oil or gas from the depths of the earth is to drill a well. Drilling rigs are used to drill holes with the help of a rotary drilling bit connected to the drill string. The drill string is driven by a hoisting system. The hoisting system consists of a wide pulley and wire system that performs operations such as lifting and lowering the drilling pipes into the well (Stan and Avram, 2015). Drilling rig brake system is a frequent braking system of heavy-duty which constantly generates frictional heat during braking processes. The disk/pad system controls the rotation of the drum to adjust the weight on the drill bit. Due to the loading conditions, the hoisting system of the rig differs from the traditional lifting machines. In the lifting machines, the load hangs in the air and does not change its weight during movement. In drilling rigs, as the depth of the well increases, the addition of each drill pipe increases the load on the hook.

During the drilling of oil and gas wells, the drilling rig is constantly active - it performs important tasks such as adjusting the speed of the drill string during raising and lowering, keeping it hanging and finally stopping it (Volchenko, 2011). Among these operations, the long-term loading of the drilling rig takes place during lifting and lowering the traveling blocks. 60-66% of the time used for total drilling operations is lifting and lowering. The loading of the brake system is due to several facts. The load may vary depending on the conditions of rapid friction, loading under the influence of force, the characteristics of the temperature distribution, the shape and size of the contact surface, the wear mechanisms and the properties of the brake pair materials.

Modern drilling rigs are powered by an electric transmission, which provides a more stable use of force and reduces vibrations (Azar and Robello, 2007). The torque is transmitted to the main drum of the drawwork by a chain drive via a hydromechanical transmission and a drive shaft. The torque applied by the chain drive and the pneumatic tire clutch activates the pulley system by rotating the drum. The lowering speed of the drill string through the pulley system is regulated by the main and auxiliary brakes consisting of the disk/pad system of the drum. A

schematic of a typical disk/pad system used for drilling rigs is shown in Figure 1. The brake mechanism mainly consists of steel or cast iron disk, brake pads, hydraulic regulator, balancer, etc. The braking force regulates the movement of the drawwork to the main drum by means of a caliper mechanism that compresses the disks through a hydraulic mechanism. The braking force using a caliper mechanism which is compressing the disks by means of a hydraulic mechanism, regulates the movement of the main drum of the drilling drawworks. A drawworks mechanism is used to control the movement of a traveling block using a pulley system (Mahboob, 2019). Drilling drawworks usually consist of the main drum and wire rope wrapped around it, main brake system, auxiliary brake system, connector disks, disk pneumatic clutch, a mechanism for tightening the fixed end of the pulley, water circulation system for cooling, drawworks carcass and a protective coating. The disk/pad brakes not only regulate the deceleration speed, but also perform the stop.

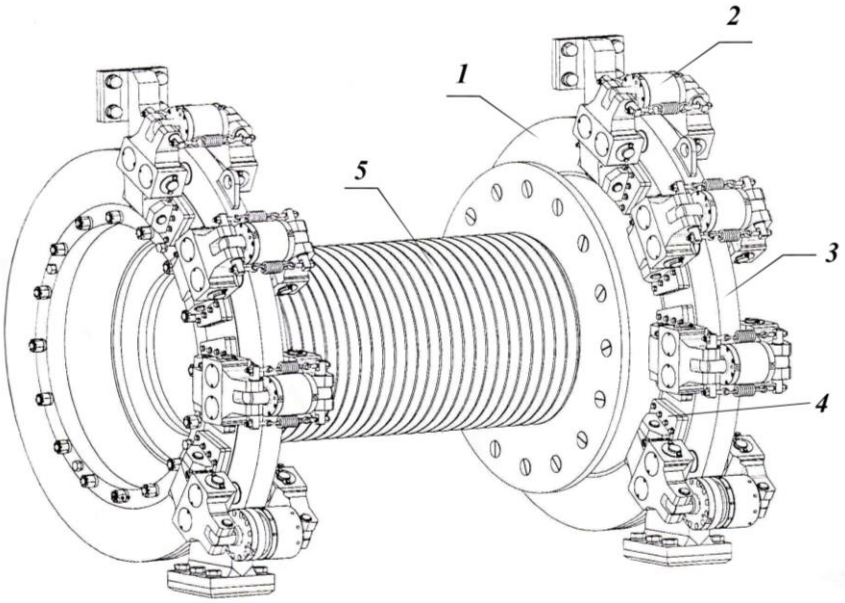

Figure 1: A schematic of the brake disk/pad system of a typical drilling rig 1) disc, 2) hydro-cylinder node (caliper), 3) support, 4) pad, 5) drum.

During the lifting and lowering of the drill string, the brake generally performs the following functions: keeping the drill string hanging while lifting the drill pipes, regulating the movement of the drill string during lowering the drill pipes, and finally stopping it. The brake is sufficiently loaded during these operations. When the drill string are lowered into the well, the pipes are added one by one and the total weight of the drill pipe column increases. As the pipes are lowered into the well, the load on the drill string increases, which causes overheating. The number of drill pipes may vary depending on the depth of the well to be drilled. A small part of the large kinetic energy generated during the process is converted into elastic deformation of the moving elements, and the main part is converted into heat between the couple elements of the brake (Drumeanu and Antonescu, 2003). Most of this heat is absorbed by the disk, and some by the brake pads which are made of various composite materials. The friction elements heat up as each drill pipe is added, and cooling occurs when the empty elevator is raised. Since the drill pipes are added one by one when the drill string is lowered into the well, its weight gradually increases, and as a result, the

lowering speed and the friction force (friction torque) also begin to change. During lifting, the speed of the drill string is reduced from 1.5...3.5 m/s to a minimum. Therefore, auxiliary brakes are used. It is important that both brakes are connected, as a large kinetic energy is generated during this process. Auxiliary braking helps to compensate for kinetic energy.

The failure of brake systems is usually due to friction and wear of pad materials due to frictional heat, which not only affects the safety of drilling, but also leads to large economic losses. Time lost during the replacement of friction pads that have lost their quality negatively affects the overall efficiency of the drilling process. The heat generated at the contact surfaces during the braking process is transferred to the environment as a result of heat transfer and radiation between the disk and the pad. Thermal changes on the surface of friction materials are very important for the brake disk and the pads. Overheating of the disk and pad causes a sharp decrease in tribological properties, and the periodic heating results in complete failure of the braking functionality (Ilyushchenko, et al., 2010). The drilling brake pad materials usually show higher wear damage in contact surfaces accompanied by high thermal stresses. High thermal stresses completely change the morphology of the contact surface and reduce the coefficient of friction to a minimum. Although drilling rigs have open or closed water cooling mechanisms, this cannot be considered as effective as desired. Because water cooling has a negative effect on the quality of the disk and significantly influence the lifetime of brake materials (Tang et al., 2011). For this reason, simulating the process of formation and distribution of frictional heat will help to better analyze the braking process.

There are numerous works in the literature devoted to the theoretical or simulation solution of the heating problem for automobiles or other friction contacts. But only a very few of them are devoted to the theoretical solution of the heating problem for the brake system of the drilling rig. Despite this, numerical studies for heat simulation of drilling brake contact, it is almost non-existent.

The aim of this paper was to simulate frictional heat generation and dissipation mechanisms during brake period. The simulations of thermal behavior of drilling brake contact surfaces, is conducted using a finite element method (FEM).

2.0 FEM SIMULATION FOR DRILLING BRAKE CONTACT

2.1 Governing Equations

Since the heat transfer problem is related to non-stationary processes, the determination of temperature distributions in the pad and the disc is solved by the differential equation of heat conduction in the cylindrical coordinate system:

$$\frac{\partial T_1}{\partial t} = a\left(\frac{\partial^2 T_1}{\partial r^2} + \frac{1}{r}\frac{\partial T_1}{\partial r}\right), 0 \le t \le t_T \tag{1}$$

The brake disc is considered to have an outer radius R_2 and an inner radius R_1. 3D calculation model for drilling brake contact is given in Figure 2. To solve the equation, the following initial and boundary conditions were used:

$$T_1(r, 0) = T_0;\ t = 0 \tag{2}$$

$$-\lambda\frac{\partial T_1}{\partial r} + q_1 = \alpha_2[T_1(R_2,t) - T_0];\ r = R_2 \tag{3}$$

$$-\lambda\frac{\partial T_1}{\partial r} = \alpha_1[T_1(R_1,t) - T_0];\ r = R_1 \tag{4}$$

The contact pressure between the disk and the pad is calculated by the following formula based on the frictional heat source P_b, per unit are (Chey et al., 2016):

$$p = \frac{P_b}{\mu\, v} \tag{5}$$

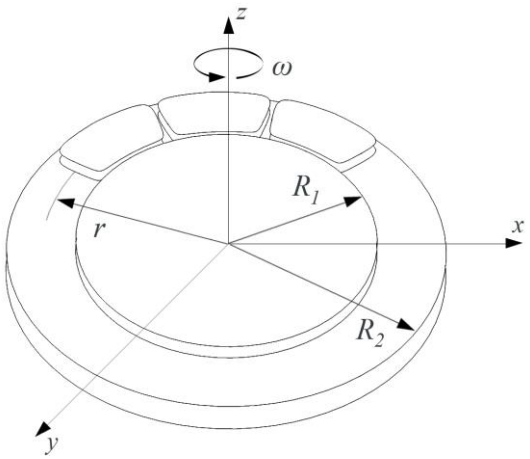

Figure 2: 3D calculation model for drilling brake contact.

The heat generated at the boundary between the disk and the brake pads is transferred to the environment by convection and radiation. The local disk velocity vector is (Shevchuk, 2009):

$$V_d = \omega\,(t)\,(-y, x) \tag{6}$$

The heat transfer in the disk and the pad interface solved by the transient heat transfer equation (Gérard, 1999):

$$\rho C_p\left(\frac{\partial T}{\partial t} + u_{trans}\cdot\nabla T\right) + \nabla\cdot(q + q_r) = Q + Q_{ted} \tag{7}$$

Thermoelastic damping can be calculated given below equation (Nowacki, 1975):

$$Q_{ted} = -\alpha T{:}\frac{dS}{dt} \tag{8}$$

Heat flux is calculated in the following sequence:

$$-n\cdot q = q_0 \tag{9}$$

From here conductive heat flux was determined thorough Fourier's law:

$$\mathrm{q} = -\mathrm{k}\nabla\mathrm{T} \tag{10}$$

And inward heat flux is calculated:

$$q_0 = h(T_{ext} - T) \tag{11}$$

The heat transfer coefficient can be calculated as follow (Limpert, 1999):

$$h = \begin{cases} 2\dfrac{k}{L}\dfrac{0.3387 Pr^{\frac{1}{3}} Re_L^{\frac{1}{2}}}{(1+\left(\frac{0.0468}{Pr}\right)^{2/3})^{1/4})} & \text{if } Re_L \leq 5 \cdot 10^5 \\ 2\dfrac{k}{L} Pr^{\frac{1}{3}}(0.037 Re_L^{\frac{4}{5}} - 871 & \text{if } Re_L > 5 \cdot 10^5 \end{cases} \tag{12}$$

A symmetry approach was used to analyze the heat along on the opposite side of the disk zone (opposite side of the contact surface):

$$-n \cdot q = 0 \tag{13}$$

The generated heat flux at the downside (d) and upside (u) boundaries during friction can be expressed as follows (Kutz, 2005):

$$-n \cdot q_d = -h\,(T_u - T_d) + rQ_b \tag{14}$$

$$-n \cdot q_u = -h\,(T_d - T_u) + (1-r)Q_b \tag{15}$$

The heat partition coefficient (thermal friction) (Yevtushenko, et al., 2011):

$$r = \frac{1}{1+\xi} \tag{16}$$

Since both bodies are made of different materials, martensite state volume fraction are calculated by the Charron equation (1942):

$$\xi = \sqrt{\frac{\rho_u C_{p,u}(k_u n_u)\cdot n_u}{\rho_d C_{p,d}(k_d n_d)\cdot n_d}} \tag{17}$$

The total heat rate (W) for produced heat (Q_1) and (Q_2) dissipated heat were calculated by equations (14) and (15).

$$W_1 = \int_0^{t_0} Q_1 dt \tag{18}$$

$$W_2 = \int_0^{t_0} Q_2 dt \tag{19}$$

The integrals are given below calculates how much of the generated heat is dissipated to the environment (air).

The thermal conductivity of brake materials is not only determined by the properties of the contacting couples. It is known that at the micro or nanoscale, surface of contacting material is usually rough. Because the surface of both solids is uneven, the gaps are filled with air (Grujicic, et al., 2005). Given that the thermal conductivity of air is much lower than that of solids, then the thermal conductivity will be lower in the non-contact regions of the brake couples. Therefore, at a microscopic level, frictional contact is made at a finite number of spots and can be expressed as (Yüncü and Kakaç, 1994):

$$h = h_c + h_g + h_r \tag{20}$$

From here the constriction conductance of two contacting surfaces can be determined by Cooper-Mikic-Yovanovich correlation (1968) according to plastic deformation of the surface asperities:

$$h_c = 1.25\, k_{contact} \frac{m_{asp}}{\sigma_{asp}} \left(\frac{\rho}{H_c}\right)^{0.95} \tag{21}$$

The values for these parameters are as follows: m_{asp} – 0.4, σ_{asp}- 1µm, h_g = 0, h_r = 0 and H_C – 850 MPa. The harmonic mean of the contacting surface conductivities:

$$\frac{2}{k_{contact}} = \frac{1}{(k_u n_u) \cdot n_u} + \frac{1}{(k_d n_d) \cdot n_d} \tag{22}$$

The heat dissipation from the contact surfaces to the environment is determined by the following equation (Kutz, 2005; Çengel and Ghajar, 2015):

$$-n \cdot q = \varepsilon\sigma(T_{amb}^4 - T^4) \tag{23}$$

2.2 Model Definition and Mesh Details

The heat model is based on the module "Heat transfer in solids (ht)" in COMSOL Multiphysics 5.5 using the finite element method. Information on the properties of friction elements, including the environment used to develop the model, is given in Table 1 (Dzhanakhmedov, et al., 2018). 35XHL steel, which is widely used in the industry, was used as the disk material and Retinax B (FK-24 A) composite was used as the brake pads.

Table 1: Different properties of friction pair materials.

Properties	**Units**	**Disk**	**Pad**	**Air**
Density	ρ (kg/m^3)	7840,0	2650,0	1.170
Special heat capacity	C_P (J/kg·K))	502.416	840,0	1100,0
Thermal conductivity	k (W/(m·K))	42,0	0.6	0.026
Surface emissivity		0.28	0.8	

The geometric dimensions of the ZJ30 drilling rig were used as a prototype. In the development of the model, the scale was reduced by ~ 3.5 times. The radius of the disk was 0.14 m, the radius of the inner cylinder was 0.096 m, and the thickness of both cylinders was 0.02 and 0.01 m, respectively. The main brake system of the ZJ30 consists of a disk and three pads (an additional one is provided for auxiliary braking). An overview of the model for the brake disk and pads is shown in Figure 3. 3D FEM model solid with shape and dimensions for the braking system consist of a disk and three pads. The maximum force on the pulley of the hoisting system is 280 kN. The maximum rotation speed of the disk is 450 rpm. In the process of heating, the heat flow affects the inner surface of the brake pads. During this time, according to Newton's law, heat exchange with the environment takes place between the surface and the inner part of the disk material. At the time of modeling, the environmental temperature was assumed to be 300K. The coefficient of friction was taken as 0.35. Heat generation during the braking process with a velocity of 10 m/s, which started at 2 secs and ended at 4 secs, and in addition, the nature of the temperature change in the disk and pad during 11 secs after braking were analyzed.

In practice, the main brake is mainly applied after the first 20-25 drill pipes are lowered, and if this process is expressed by a trapezoidal tachogram, we obtain a graph consisting of three stages (Zhuravlev, 2016; Vanitsky, 1978). Figure 4 shows the process of releasing a loaded elevator ($t_{r.e}$) for a drilling rig into a well, which describes changing the speed at different stages. Phase I involves the start speeding up (v_s), phase II involves the regulation of uniform velocity, and stage III involves the process of stopping the lowered column through the friction knots of the drilling rig. The change in friction moment (M_f) according to the mentioned stages is also shown in the graph. After the maximum speed ($v_{s\,max}$) is reached due to inertia, the process of regulating the movement through the brake system is carried out for a short period of time. Since the process of frictional heat generation occurs mainly during the load increase, the heating model is linked to phase III of the tachogram.

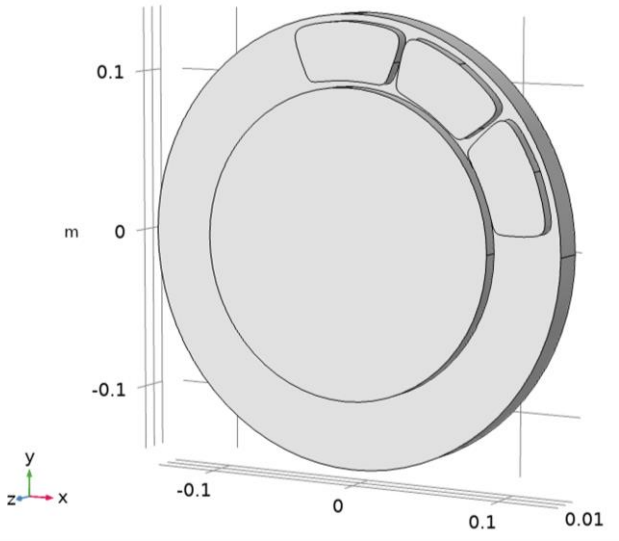

Figure 3: Three-dimensional model for the brake disk/pad couple.

The mesh model is composed of with a mainly triangles elements and a total degree of freedom (DOF) of 110866 (Figure 5). A grid sensitivity test was applied to ensure the sufficiency of the meshing scheme and grid independence. A grid independence test was applied by several mesh iterations with the convergence criteria set at 10^{-6}. A mesh independence study showed that mesh characteristics are less than 2% error. It was established a maximum element size of 24800. Details of mesh model properties are presented in Table 2.

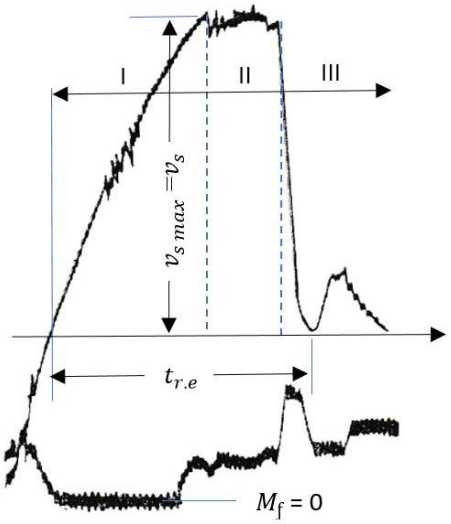

Figure 4: The change in speed during the lowering of the drill string along the length of the pipe.

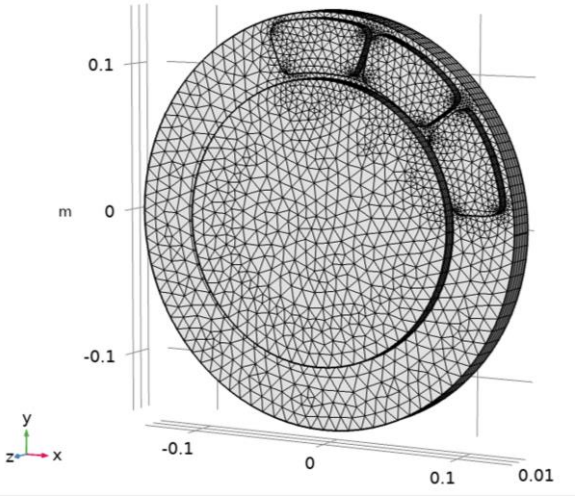

Figure 5: Mesh model for disk and brake pads.

The contact pressure between the friction pair materials is related to the frictional heat per unit area. The heat generated at the contact boundary between the disk and the pad is transferred to other elements of the brake system by convection and radiation. Physical processes such as heat transfer within solids, heat flux, heat exchange during thermal contact, and radiation of heat from contact surfaces to the environment were studied and the results obtained were reflected in the final model.

Table 2**:** Details of finite element mesh model

Models	**Materials**	**Number of elements**	**Mesh volume (m^3)**
Disk	Steel 35XHL	24800	0.001578
Pad	Retinax B (FK24A)	4070	$5.776 \cdot 10^{-5}$

3.0 RESULTS AND DISCUSSION

The results of the thermomechanical model are visualized and shown in Figures 6 and 7. To ensure the accuracy of the obtained results, a comparison of the simulation results with experimental results was made. In these studies, it was found experimentally that the temperature rises to 1270-1550K depending on the counter-body materials and friction regimes, which is close to conducted numerical analysis (Wang, 2008; Volchenko, 2019). From the shown images, it is possible to observe how the frictional heat is distributed on the contact surface of the friction pair materials during braking, depending on the time. As can be seen from the images, the heat generated along the friction path created by the disk in the contact area with the pad, and distributed to other areas of the disk as the rotational movement continued. In braking, the process became more intensive. After 2.65 sec, it is possible to see the temperature rise on the upper surface of the brake pads. Looking closer at the contact between the disk and the brake pads, we see that the heat is directed in the opposite direction from the point of intersection (up and down directions) of both friction elements (Figure 6 a,b).

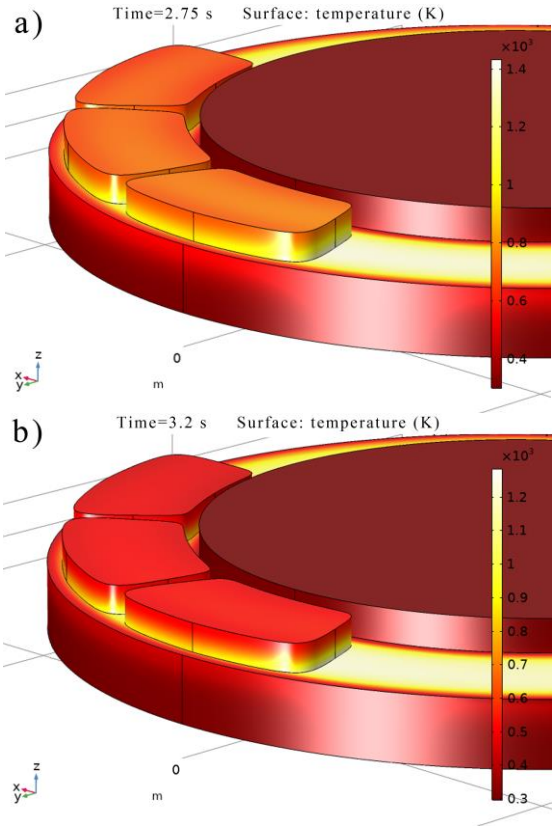

Figure 6: Temperature distribution on the contact surface in a) 3.2 sec and b) 2.75 sec.

However, as is clear from the given observations, the fact that the heat spreads faster inside the brake pad and heats up should be understood as a significant difference between the dimensions of the material and its thermal properties. After about 5 secs, the surface temperature of the pads began to change around 1000 K (Figure 7 d, e, f). In general, the highest temperature is the was found first 2-4 secs (Figure 7 b, c, d). Thus, at 3.85 sec, the temperature was 1540 K. After the braking process was completed, the cooling process took place on the surface of the disk and reached 500-600 K at the end of 15 secs. Also, the temperature was lower in the parts close to the center compared to the outer parts of the disk.

In general, in the part along the surface of the middle element of the disk was last heated part. The temperature in this part usually varied in the range of 300-400 K. Figure 8 a, b shows the distribution of heat from the opposite part of the contact surface. As can be seen from both images, the temperature was lower in the center of the disk, the temperature rose at the edges of the disk during braking, and in the next stage it gradually began to decrease.

Thus, in both cases, the temperature was relatively low in the central part of the disk and remained stable at ~ 300-400 K. To determine the temperature profile of the contact area for the the position of the hotspot between brake pad and rotating disk, a line is drawn from the center of the disk to the pads edge and an angle field is created with the point marked by the red arrow in Figure 9.

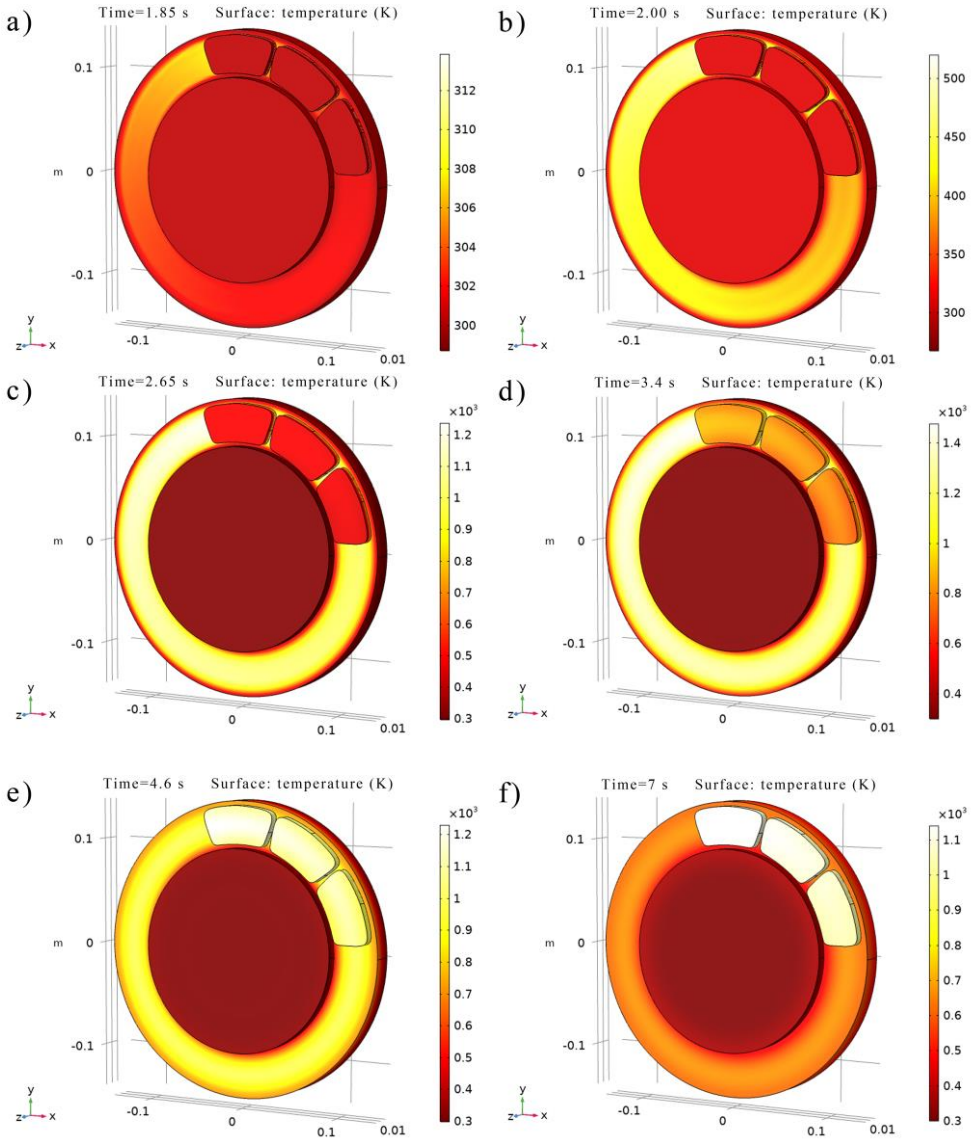

Figure 7: Temperature change during different braking conditions: a) 1.85 sec, b) 2.00 sec, c) 2.65 sec, d) 3.40 sec, e) 4.60 sec, f) 7.00 sec.

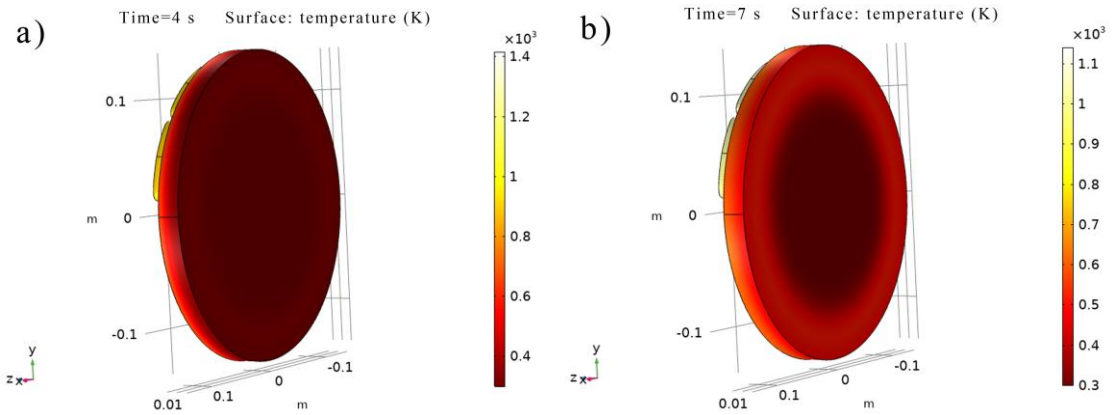

Figure 8: Temperature distribution on the opposite side of the contact surface in a) 4 sec and b) 7 sec.

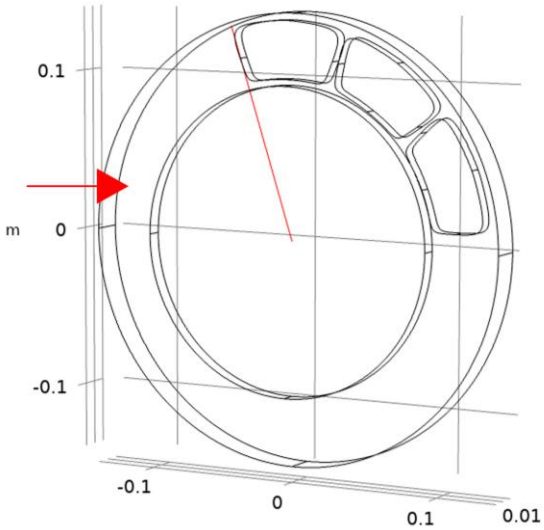

Figure 9: The radial line for temperature profile of disk surface.

The graph obtained for the temperature profile is presented in Figure 10. As can be seen from the graph, the temperature rise starts at 2 sec, reached a maximum during for 3-4 sec., and then began to partially decrease. At this time period temperature continued to rise to ~ 1400 K then a decrease was observed. After 7 secs, temperature distributed more uniformly along the surface of the rotating disk. As the braking continued, the brake pads also began to heat up and reached a temperature of ~1400-1500 K at the end of the analysis. When two solids come into contact with each other, heat is released as a result of the formation and destruction of friction bonds under the influence of elastic or plastic deformation. At the microscopic level, the contact of materials takes place in real contact zones, and the resulting heat is transferred from the high temperature area to the low temperature area. Because brake pads usually have a heterogeneous structure, the distribution and effect of heat vary depending on the thermo-mechanical properties of the components. However, as the process is repeated, the heat is gradually distributed inside the

material, which reduces physical and mechanical properties. As a result of changes in the friction surface, the frictional force between the applied contact materials decreases, and thus the coefficient of friction decreases (Bijwe and Mazumdar, 2006).

As can be seen in Figures 6 and 8, the heat distribution within the material gradually became homogeneous after the braking phase. This suggests that continuous sliding in heavily loaded systems, such as drilling rig brakes, have a significant impact on the change of tribological characteristics of materials.

The formation of thermal stress and deformation on the surface of the disk occurs due to a sharp drop in temperature in the radial and axial directions. The temperatures on the inner and outer surfaces of the disc differ sharply. An axial drop in temperature on the surface of the disc causes thermal stress and deformation (Adamowicz, 2016). The pressure is usually distributed in proportion to the radius. However, due to the roughness of the contact surfaces, the formation and release of heat have a very different effect on the wear and thermal properties.

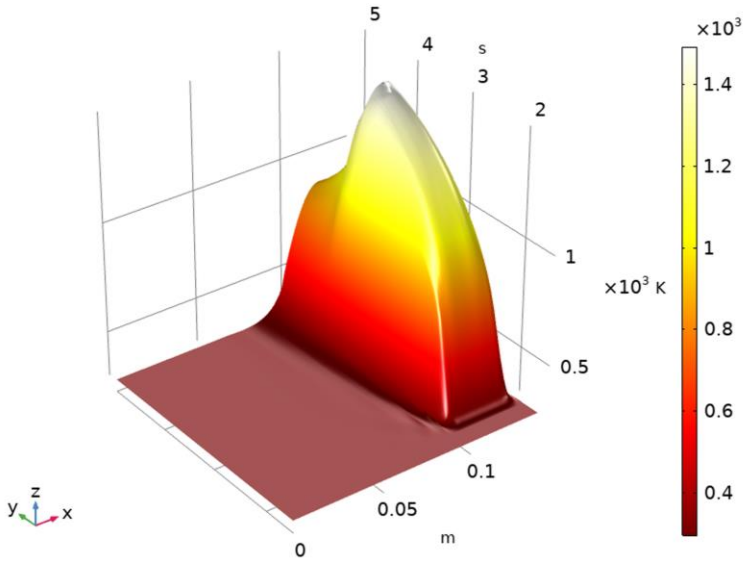

Figure 10: Temperature profile for disk surface.

At the end of the brake, the heat is already enters throughout the material and temperature distributed over the entire volume. As the drill string is lifted, as the surface remains exposed, the contact surface begins to cool more rapidly, resulting in tensile stresses. Tensile stresses cause the formation of microcracks on contact surfaces. Observations of the wear surfaces show that the cracks on the contact surface are perpendicular to the direction of sliding, and on the inner cracks in the direction of sliding. This mainly depends on the physical and chemical properties of the material and the temperature distribution. This means that the loading of the disc and pad is irregular and variable, not only in the radial direction, but also in the axial direction.

Results for calculations of the total heat rate (W) for produced heat (Q_1) and (Q_2) dissipated heat using integrals were given in Figure 11. Obtained plots show that how much of the generated heat is dissipated to the environment as a function of time for the disk material.

As can be seen from the graph, the amount of total produced heat began to increase under the influence of friction between the contact surfaces after 2 sec, and remained stable after 3-4 secs.

The dissipated heat became more intense after 3-4 secs, in accordance with the produced heat. The increase in dissipated heat after this period can be understood as the transfer of more heat to the environment due to the heating of the friction elements. However, if the braking is repeated, the amount of heat transferred to the environment is equal to the amount of heat generated during braking. In this case, the temperature of the friction surface will be the same at the end of each braking.

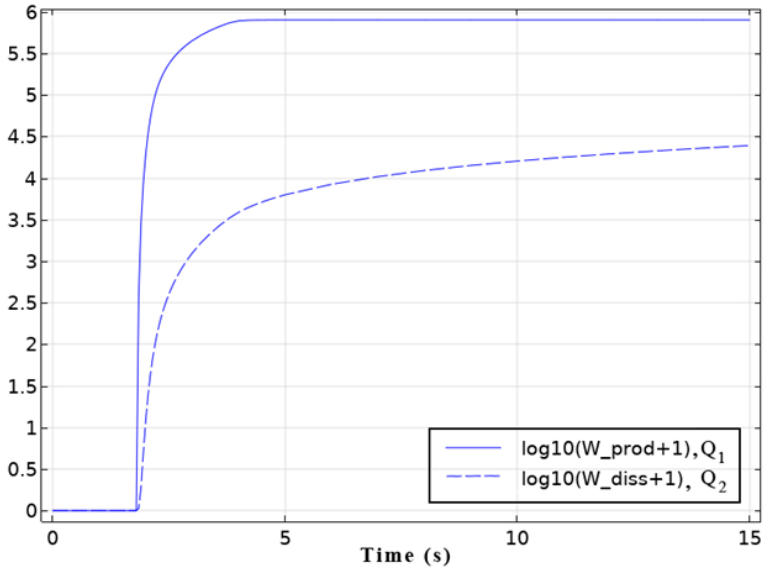

Figure 11: Comparison of total produced heat and dissipated heat.

CONCLUSIONS

In this study, heat distribution in a drilling disk brake and pad contact have been modeled and analyzed by a finite element approach. The results obtained for drilling brake contact surface temperatures of the pad and the disk show that the friction surfaces are significantly heated within the given brake time phase and the following main results were obtained:

The temperature on the surface of the brake pads began to rise rapidly after 2.65 secs. The highest temperature was found first 2-4 secs. The highest disk surface temperature was observed at 3.85 sec, in this time period temperature was 1540 K. The surface temperature of brake pads reached a temperature of ~1400-1500 K at the end of the analysis. 4-7 secs after the end of braking, the temperature on the surface of the disk gradually decreased and a uniform distribution of heat along the surface was observed.

Based on the results obtained, parameters such as load, sliding velocity, friction coefficient and surface roughness of brake disk and pad affecting the heat generation and dissipation can be investigated.

REFERENCES

Adamowicz, A. (2016). Finite element analysis of the 3-D thermal stress state in a brake disk. Journal of theoretical and applied mechanics, 54 (1), 205-218.

Azar, J.J., & G. Robello, S. (2007). Drilling Engineering. PennWell Books.

Bijwe, N.J., & Mazumdar, N. (2006). Influence of amount and modification of resin on fade and recovery behavior of non-asbestos organic (NAO) friction materials, Tribology letters, 23(3), 215-222.

Çengel, Y.A., & Ghajar, A.J. (2015). Heat and mass transfer fundamentals and applications, Mc Graw-Hill Education.

Chey, S.K., Tian, P., Tian, Y. (2016). Estimation of real contact area during sliding friction from interface temperature. AIP Advances, 6 (6), 065227.

Drumeanu, A.C., & Antonescu, N.N. (2003). The drilling draw-works band brakes thermal regime. National Tribology Conference. Pp.147-152.

Dzhanakhmedov, A.Kh, Pirverdiev, E.S, Volchenko, A.I. (2018). Friction units in mechanical engineering (in Russian). Baku. Elm.

Gérard, M. (1999). The thermomechanics of nonlinear irreversible behaviors: An introduction. World Scientific.

Grujicic, M., Zhao, C.L., Dusel, E.C. (2005). The effect of thermal contact resistance on heat management in the electronic packaging, Applied surface science, 246 (1–3), 290-302.

Ilyushchenko, .F., Dmitrovich, A.A., Saroka D.I. et al. (2010) Sintered friction composite materials and products: 50 years of powder metallurgy in Belarus. History, achievements, prospects. Minsk. (in Russian).

Kutz, M.P. (2005). Heat transfer calculations, McGraw-Hill Professional.

Limpert, R. (1999). Brake design and safety, Second edition. Society of automotive engineers, USA.

Mahboob, K., Ahmad, A., Mushtaq, U. et al. (2019). Design and analysis of the structure of a drill rig. Pakistan journal of science, 71 (4), 2019. 119-125.

Nowacki, W. (1975). Dynamic problems of thermoelasticity. Nordhoff international publishing.

Shevchuk, I.V. (2009). Convective heat and mass transfer in rotating disk systems. Springer.

Stan, M., & Avram, L. (2015). Experimental study on the model of the correlation between the movement of the drilling string with big diameter of drill and effects on the oil rigs. Journal of Petroleum Exploration and Production Technology, 5, 295–303.

Tang, W. X., Cai, Y. D., Cheng, C., & Huang, Q. Y. (2011). Thermal stress analysis of water-cooling brake disk based on 3D thermo-mechanical coupling model. Advanced materials research, 314-316.

Vanitsky, M.M. (1978). Rational control of round-trip operations, Nedra (in Russian).

Volchenko, D.A. (2011). Brakes with cooling of the "heat pipe" type. Exploration and Development of Oil and Gas Fields, 3(40), 17-26. (in Russian).

Volchenko, A. I., Skrypnyk, V.S., Popovych, V. Ya et al. (2019). Assessment of patterns of change in operational parameters of friction pairs of brake devices. Problems of friction and wear, 4 (85), 53-60

Wang, X., Wang, S., Zhang, S., et al. (2008). Wear mechanism of disc-brake block material for new type of drilling rig. Frontiers of mechanical engineering, 3(1),10–16.

Yevtushenko, A., & Grzes, P. (2011). Finite element analysis of heat partition in a pad/disk brake system. Numerical heat transfer, Part A: Applications, 59(7), 521–542.

Yüncü, H., & Kakaç, S. (1994). Thermal contact conductance - Theory and applications. Cooling of electronic systems. NATO ASI series (Series E: Applied Sciences), 258, 677-702.

Zhuravlev, D., Yu. (2016). Calculation and design of friction units of a band-shoe brake. Interuniversity collection "Scientific notes". 55, 152-156. (in Russian).